ChemPubSoc Europe

DOI: 10.1002/chem.201601505

CHEMISTRY A European Journal Full Paper

Hydrogen Bonds

Exploring the Strength of the H-Bond in Synthetic Models for Heme Proteins: The Importance of the N–H Acidity of the Distal Base

Mariza N. Alberti,[a] Yevhen Polyhach,[b] Manolis D. Tzirakis,[a] Laura Tödtli,[b] Gunnar Jeschke,*[b] and François Diederich*[a]

Dedicated to Professor James P. Collman

Abstract: The distal hydrogen bond (H-bond) in dioxygen-binding proteins is crucial for the discrimination of O_2 with respect to CO or NO. We report the preparation and characterization of a series of Zn^{II} porphyrins, with one of three *meso*-phenyl rings bearing both an alkyl-tethered proximal imidazole ligand and a heterocyclic distal H-bond donor connected by a rigid acetylene spacer. Previously, we had validated the corresponding Co^{II} complexes as synthetic model systems for dioxygen-binding heme proteins and demonstrated the structural requirements for proper distal H-bonding to Co^{II}-bound dioxygen. Here, we systematically vary the H-bond donor ability of the distal heterocycles, as predicted based on pK_a values. The H-bond in the dioxygen adducts of the Co^{II} porphyrins was directly measured by Q-band Davies-ENDOR spectroscopy. It was shown that the strength of the hyperfine coupling between the dioxygen radical and the distal H-atom increases with enhanced acidity of the H-bond donor.

Introduction

Myoglobin (Mb) and hemoglobin (Hb) are heme proteins whose physiological importance is principally related to their ability to bind, transport, and store dioxygen. The binding pocket of these proteins contains an iron protoporphyrin IX, which is designated as heme (Fe^{II}) or hemin (Fe^{III}).[1] The Fe^{II} atom is coordinated to the heme through four pyrrole nitrogens and to the protein moiety through a proximal histidine. On the other side of the heme, in the so-called distal pocket, three strongly conserved residues are in close proximity: phenylalanine, valine, and most importantly histidine. In this pocket, the Fe^{II} atom can efficiently bind O_2, CO, and NO, which is of critical importance to physiological processes such as respiration, neurotransmission, and vasodilation.[2] A common feature shared by all heme proteins is their enhanced affinity for O_2 over CO or NO. There is great interest in understanding the fundamental principles of how the heme distal pocket favors O_2 binding. In fact, the elucidation of the mechanism responsible for this molecular recognition process has been a matter of some controversy.[3] Pauling initially suggested that the distal histidine stabilizes bound dioxygen by a H-bonding interaction.[4] A series of EPR,[5] resonance Raman,[6] NMR,[7] neutron diffraction analysis,[8] X-ray,[6b,9] as well as rapid mixing and laser photolysis[10] studies supported the presence of such an interaction ("Pauling hypothesis").

Previously, a suitable pulse EPR method was described to directly determine the nature, the orientation, as well as the length of the H-bonding interaction between the distal side residue and bound dioxygen in **Co-Mb-O_2** and in model complex **1-Co-O_2** (Figure 1).[11] As an extension of our studies in this area, we also examined the geometrical prerequisites for the H-bonding interaction in a series of synthetic models for heme proteins.[12] These prerequisites were found to be narrow and very specific. Among the studied complexes, **1-Co-O_2** possessed ideal distal constitution to form this interaction and hence is regarded as an excellent model for the binding pocket of Mb and Hb. The aim of the present study is to shed further light onto the strength of the vital H-bonding interaction by systematically varying the N–H acidity of the distal base in the series **1**–**8-Co-O_2** (Figure 1) and directly investigating the effect of these changes on the dioxygen-binding pocket by NMR and Q-band Davies-ENDOR (Electron-Nuclear DOuble Resonance) spectroscopies.

[a] Dr. M. N. Alberti, Dr. M. D. Tzirakis, Prof. Dr. F. Diederich
Laboratorium für Organische Chemie, ETH Zurich
Vladimir-Prelog-Weg 3, 8093 Zurich (Switzerland)
E-mail: diederich@org.chem.ethz.ch

[b] Dr. Y. Polyhach, L. Tödtli, Prof. Dr. G. Jeschke
Laboratory of Physical Chemistry, ETH Zurich
Vladimir-Prelog-Weg 2, 8093 Zurich (Switzerland)
E-mail: gunnar.jeschke@phys.chem.ethz.ch

Supporting information for this article is available on the WWW under http://dx.doi.org/10.1002/chem.201601505.

© 2016 Wiley-VCH Verlag GmbH & Co. KGaA, Weinheim

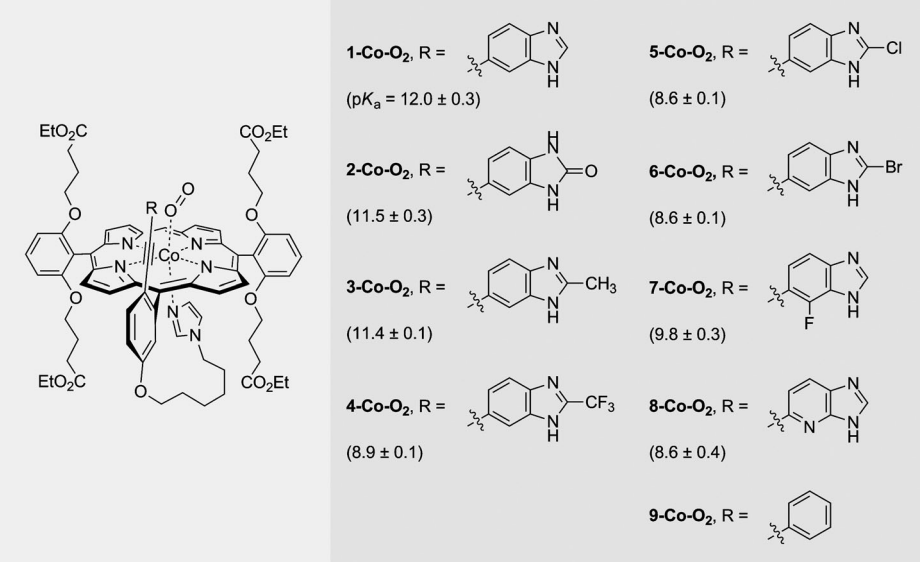

Figure 1. Model compounds **1**–**9-Co-O$_2$** for pulse EPR investigations. The values in parenthesis are the ACD-calculated pK_a[13] values for the phenylacetylene derivatives of the distal bases in **1**–**8-Co-O$_2$**.

Results and Discussion

Porphyrin synthesis

For the purpose of the present study, we prepared a series of seven novel model complexes **2**–**8-Co-O$_2$** endowed with different distal bases. Figure 1 depicts their structures along with the estimated pK_a values, calculated by the ACD/pK_a software[13] for the phenylacetylene derivatives of the distal bases, in parenthesis. The last model complex, **9-Co-O$_2$** (Figure 1), was synthesized from the precursor porphyrin **9-Zn**, a fully characterized by-product of the Sonogashira cross-couplings under the conditions assessed in this study (vide infra).

The synthesis of porphyrins **1**–**9-Co** is outlined in Scheme 1. Porphyrin **10-Zn** is the common precursor of these porphyrins

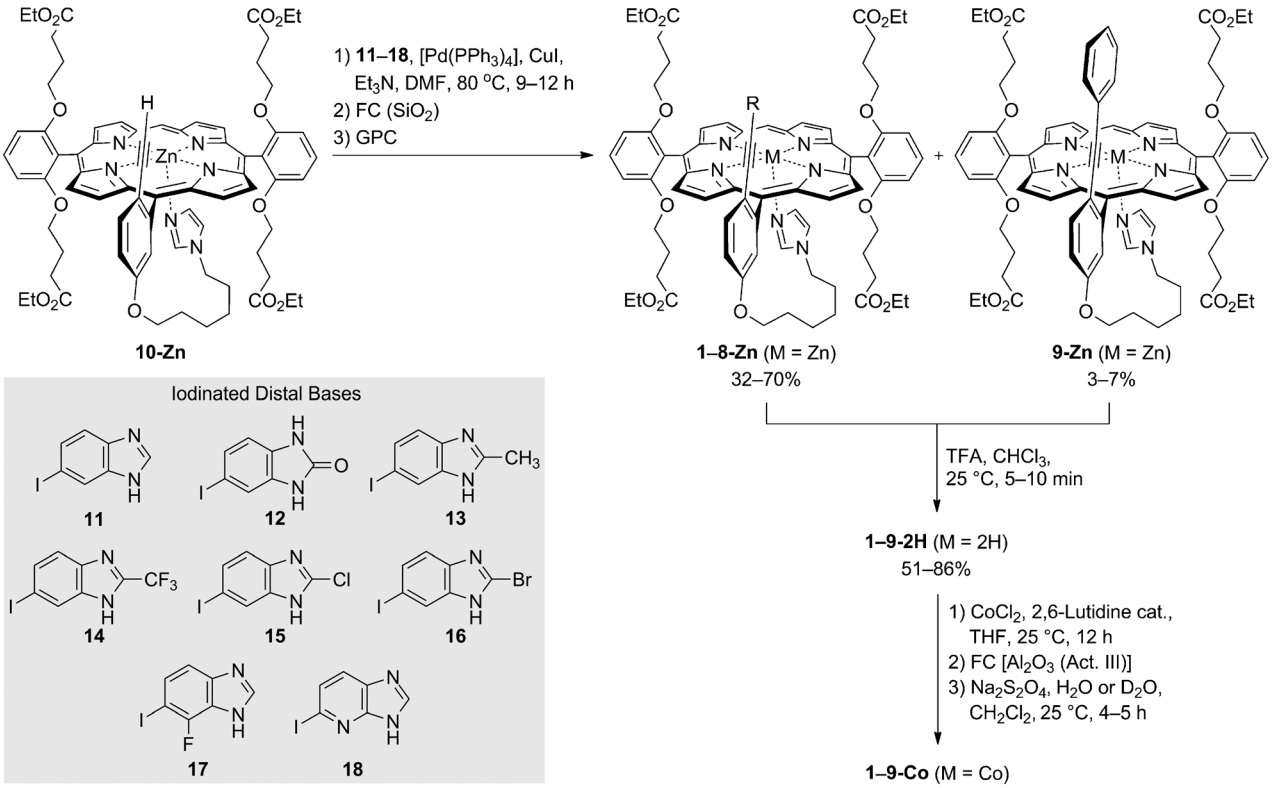

Scheme 1. Synthesis of model compounds **1**–**9-Co**. DMF = dimethylformamide, FC = flash chromatography, GPC = gel permeation chromatography, TFA = trifluoroacetic acid, THF = tetrahydrofuran.

© 2016 Wiley-VCH Verlag GmbH & Co. KGaA, Weinheim

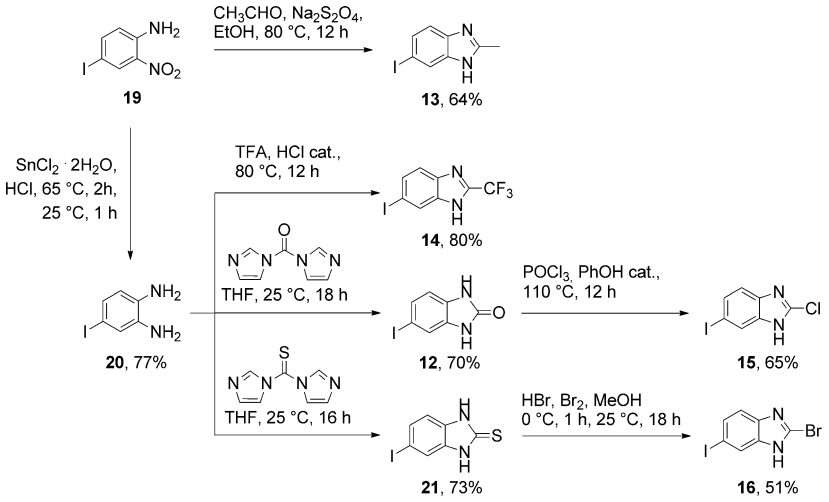

Scheme 2. Synthesis of iodinated distal base precursors **12**–**16**. TFA = trifluoroacetic acid, THF = tetrahydrofuran.

and its synthesis is described in the literature[11,12] and—upon addition of new findings—in Section S2.1 of the Supporting Information. Sonogashira cross-coupling of **10-Zn** with compounds **11**–**18** in the presence of $[Pd(PPh_3)_4]$ as a catalyst afforded porphyrins **1**–**8-Zn** in satisfactory yields (32–70%).[14] Interestingly, in all cases, in addition to the desired porphyrins **1**–**8-Zn**, the unanticipated by-product **9-Zn** was also formed and fully characterized by 1D/2D NMR techniques as well as mass spectrometry. Porphyrin **9-Zn** is formed by phenyl-aryl exchange during the cross-coupling reaction (aryl = distal base; phenyl derives from $[Pd(PPh_3)_4]$);[15] a plausible mechanism[16] for the formation of this porphyrin is provided in Section S2.2 of the Supporting Information. In the next step, the Zn^{II} ion was removed with trifluoroacetic acid (TFA) affording porphyrins **1**–**9-2H** in moderate to high yields (51–86%). Surprisingly, these free-base porphyrins were stable at ambient conditions, which allowed for their characterization by 1D/2D NMR techniques as well as by mass spectrometry. Subsequently, Co^{II} was inserted into the free-base porphyrins **1**–**9-2H** using $CoCl_2$; this reaction was conducted in a glovebox. In all cases, the Co^{II} insertion provided a mixture of both Co^{II} and Co^{III} porphyrins, as was evidenced by their UV/Vis spectra.[17] Thus, an additional reduction with an aqueous solution of $Na_2S_2O_4$ was performed in the glovebox, affording the desired Co^{II}-containing complexes.

The synthesis of the precursors to the distal bases, **12**–**16**, is presented in Scheme 2. Specifically, the preparation of 5-iodo-2-methyl-1*H*-benzimidazole (**13**) was achieved in one step by the $Na_2S_2O_4$ reduction of 4-iodo-2-nitroaniline (**19**)[18] in the presence of acetaldehyde.[19] Reduction of aniline **19**,[18a,20] followed by treatment with TFA in the presence of catalytic HCl, gave 5-iodo-2-(trifluoromethyl)-1*H*-benzimidazole (**14**) in 62% overall yield.[21] 5-Iodo-1,3-dihydro-2*H*-benzimidazol-2-one (**12**) was obtained by treatment of 4-iodobenzene-1,2-diamine (**20**) with 1,1′-carbonyldiimidazole.[22] Subsequently, distal base **12** was reacted with $POCl_3$ and a catalytic amount of phenol to afford 5-iodo-2-chloro-1*H*-benzimidazole (**15**) in 35% overall yield.[22,23] Finally, 5-iodo-2-bromo-1*H*-benzimidazole (**16**) was synthesized by treatment of 5-iodo-1,3-dihydro-2*H*-benzimidazole-2-thione (**21**) with HBr/Br_2 in MeOH.[24] Compound **21** was synthesized by the thiocarbonylation of 4-iodobenzene-1,2-diamine (**20**) using 1,1′-thiocarbonyldiimidazole.[25]

The synthesis of benzimidazole **17** proceeded in three steps (Scheme 3). Iodination of 3-fluoro-2-nitroaniline (**22**)[26] with iodine monochloride[18] gave a mixture of two regioisomers **23** and **24** in 19% and 63% yield, respectively. It is worth noting that in the course of this reaction, a less polar compound was also isolated (3–4%), the structure of which could not be determined based on 1D/2D NMR techniques as well as HR-MS spectrometry. Reduction of compound **24** with $SnCl_2{\cdot}2H_2O$ and 12 N HCl in MeOH[27] afforded 3-fluoro-4-iodobenzene-1,2-diamine (**25**) in 88% yield. Due to the instability of diamine **25** at 25 °C, this compound was used directly in the subsequent reaction without further purification. Accordingly, cyclization of crude diamine **25** in the presence of formic acid[28] gave distal base precursor **17** in 73% yield. The synthesis of precursor **18**

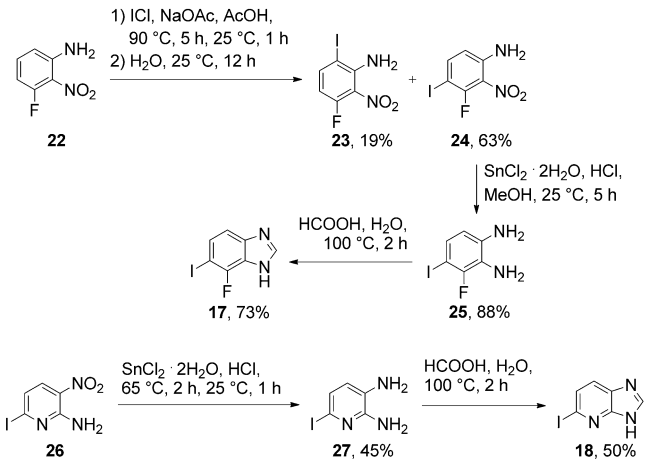

Scheme 3. Synthesis of iodinated benzimidazoles **17** and **18**.

© 2016 Wiley-VCH Verlag GmbH & Co. KGaA, Weinheim

was carried out in a similar manner (Scheme 3). Specifically, 6-iodo-3-nitropyridin-2-amine (**26**)[29] was treated with $SnCl_2{\cdot}2H_2O$ and 12 N HCl[18a,20] to afford 6-iodopyridine-2,3-diamine (**27**) in 45% yield. Subsequent cyclization of diamine **27** in the presence of formic acid[28] gave **18** in 50% yield.

Conformation of zinc complexes in $CDCl_3$ solution at 25 °C

The conformations of the proximal and distal site residues of the different models **1**–**9**-**Zn** in solution were investigated by NMR spectroscopy.

Regarding the proximal site of porphyrins, for model complexes **1**–**6-Zn** and **9-Zn** the ^{1}H NMR resonances of the hexyl-tethered imidazole moieties are significantly upfield shifted, appearing at $\delta = 1.97$–2.09 (position 5), 2.22–2.59 (position 2), and 4.91–5.30 ppm (position 4; Figure 2). This observation is indicative of axial imidazole ligation to the Zn^{II} ion;[30] upon ligation, the imidazole protons are exposed to the shielding region of the strong aromatic ring current of the porphyrin. On the other hand, the aforementioned upfield-shifted signals are not clearly visible in the ^{1}H NMR spectra of **7-Zn** and **8-Zn** at 25 °C (Supporting Information, Figure S59 and S67). In the ^{1}H NMR spectra of **7-Zn**, a peak broadening throughout the spectral range is observed. In addition, the comparison of the ^{1}H NMR spectra of **7-Zn** or **8-Zn** at 40 °C and −40 °C (Supporting Information, Figure S65 or S72) showed new signals in the range of $\delta = 1.8$–2.6 and 4.5–6.0 ppm, which could be explained by the convergence of various conformers of **7-Zn** or **8-Zn** to more stable ones. In these two model complexes, it seems reasonable to assume that there is a dynamic equilibrium between the ligation of hexyl-tethered imidazole and alkyne-appended benzimidazole to the Zn^{II} ion (with rates that are comparable to the NMR timescale) and that the axial ligation of proximal imidazole to the Zn^{II} ion is favored at lower temperatures.

Regarding the preferred orientation and tautomeric state of the distal bases, after vigorously shaking a solution of **1-Zn**, **2-Zn**, and **4**–**6-Zn** in $CDCl_3$ with D_2O for 10 s, ^{1}H NMR spectra

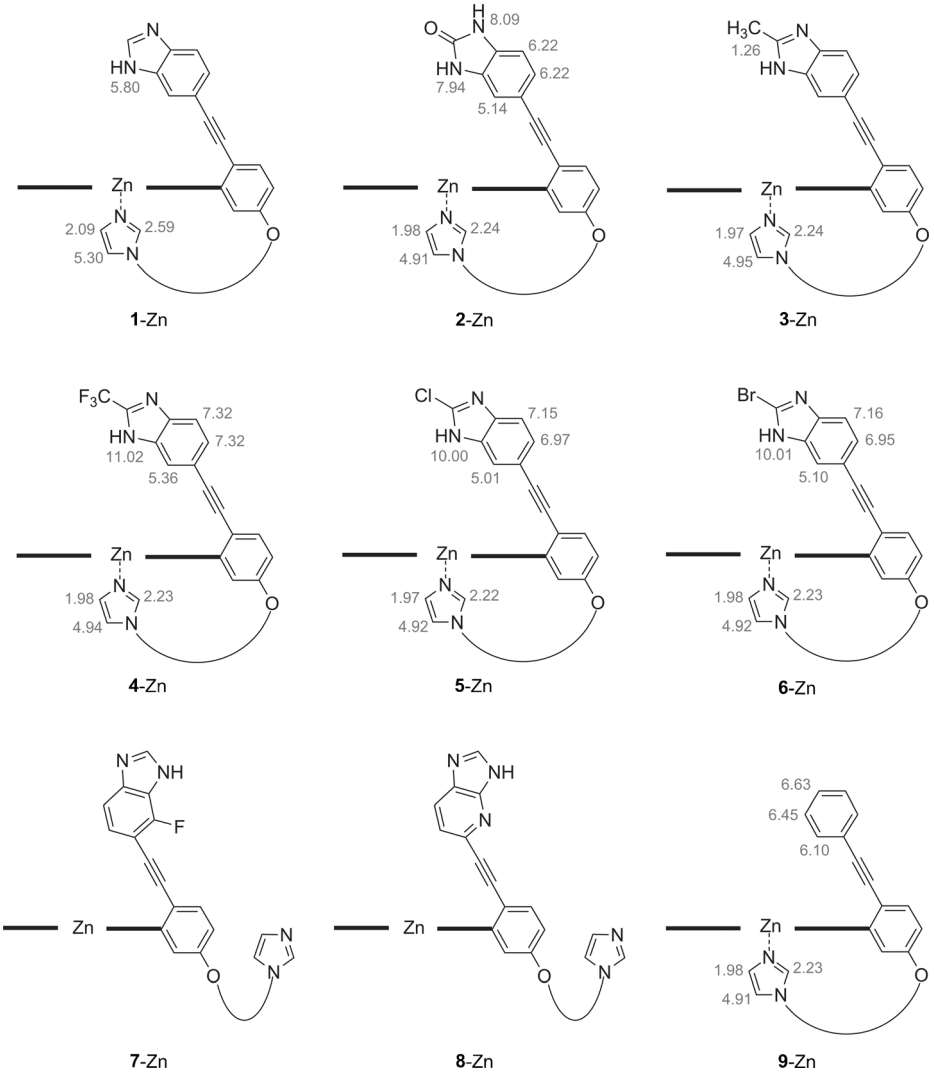

Figure 2. Schematic view of the preferred conformations of model complexes **1**–**9-Zn** in solution ($CDCl_3$, 25 °C) as determined by ^{1}H NMR spectroscopy. Indicative proton chemical shifts are given in ppm (chemical shifts for complex **1-Zn** were taken from Ref. [11]). Certain residues of the molecules were omitted for clarity.

© 2016 Wiley-VCH Verlag GmbH & Co. KGaA, Weinheim

showed the disappearance of NH signals (assignments of these signals (ppm values) are shown in Figure 2). In all cases, these NH signals are shifted upfield. The range of the upfield shift is $\delta = 2.61–6.72$ ppm, as compared to the NH resonances of the corresponding iodinated bases (**11**, **12**, and **14**–**16**; Scheme 1). This upfield shift indicates the proximity of the NH proton to the porphyrin π-cloud. Thus, it can be concluded that the distal base NH moieties in complexes **1-Zn**, **2-Zn**, and **4**–**6-Zn** are turned towards the porphyrin plane and, especially in complexes **1-Zn** and **4**–**6-Zn**, only the tautomers with the NH proton pointing towards the porphyrin plane are present in solution. The preferred conformations of the aforementioned complexes are shown in Figure 2. This structural assignment is further supported by the resonances of the aromatic protons in the distal bases of **2-Zn**, and **4**–**6-Zn** (Figure 2). Presumably, the proposed conformations are stabilized by N–H···π interactions of the exchangeable distal protons with the porphyrin chromophore.[31] Due to the broadness and weakness of benzimidazole peaks in complexes **3-Zn**, **7-Zn** and **8-Zn**, direct assignment of these proton resonances was not possible. For complexes **7-Zn** and **8-Zn**, the distal bases are probably rotated outwards, away from the porphyrin plane, because of electrostatic repulsion between the porphyrin π-cloud and the F-atom or the N4 lone pair of the substituted benzimidazoles.

H-Bond strength between the distal residue and bound oxygen in 1–8-Co-O_2 species by Q-band Davies-ENDOR spectroscopy

Prior to the Q-band Davies-ENDOR experiments, field-swept ESE (electron spin echo)-detected spectra were taken for **1**–**8-Co-O_2** complexes. These ESE spectra were used to select the observer positions for acquisition of the Davies-ENDOR spectra and determine the *g*-tensors needed for the simulations of Davies-ENDOR spectra. The ESE spectrum of **6-Co-O_2** is shown in Figure 3 A, whereas the ESE spectra of **1**–**5-Co-O_2** and **8-Co-O_2** complexes are included in the Supporting Information (Section S5.2, Figures S175–S182 A, respectively); as mentioned below, a stable, oxygenated **7-Co-O_2** complex could not be obtained.

Principal values of the electronic *g*-tensors of **1**–**6-Co-O_2** and **8-Co-O_2** complexes, determined by EasySpin simulations, are presented in Table 1. The set of the Davies-ENDOR spectra for **6-Co-O_2** acquired at many observer positions is shown in Figure 3 B. Such sets of spectra for the remaining complexes are shown in the Supporting Information (Section S5.2, Figures S175–S182). Note that these spectra are very rich in information as they feature resonance bands stemming from many coupled protons in **1**–**6-Co-O_2** and **8-Co-O_2**. In the present study, we focused only on the strongest coupling that corresponds to the exchangeable proton of the distal base.[11,12] Spectral features associated with that coupling are indicated by arrows in Figure 3 B. The set of Davies-ENDOR spectra acquired at different observer positions contains information about the strength of the hyperfine coupling as well as the relative orientation of the hyperfine coupling tensor and the electronic *g*-tensor, which can be extracted by means of rigorous

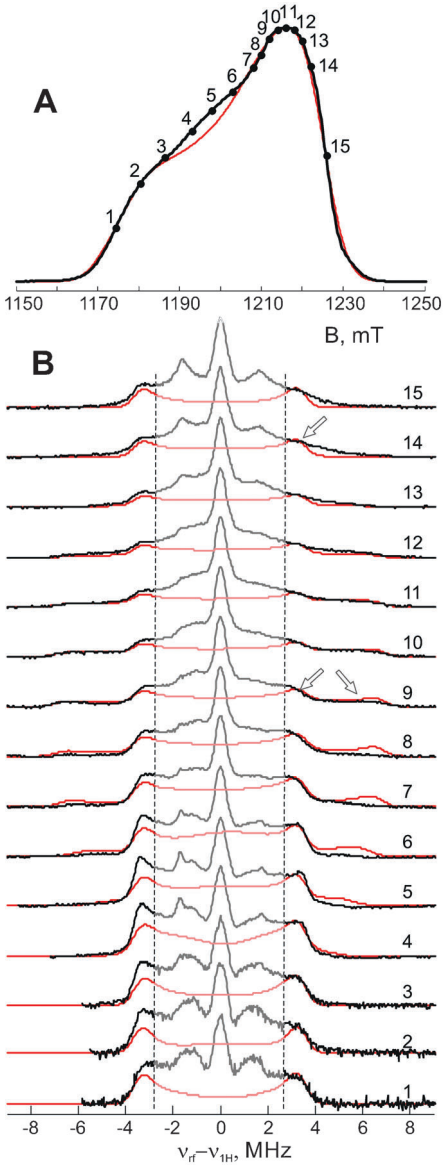

Figure 3. Experimental EPR spectra for **6-Co-O_2** (Q band, 10 K). A) Magnetic field swept ESE spectrum (black) superimposed with the EasySpin simulation (red). Black circles with numbers on the ESE spectrum denote observer positions on which Davies-ENDOR spectra were acquired. B) Experimental Davies-ENDOR spectra (black) superimposed with the EasySpin simulation (red). Arrows denote spectral regions were resonances due to the strongly coupled proton occur.

spectra simulations. A complete example of such analysis is given for **1-Co-O_2** (for which we observed the most prominent resonance bands from the exchangeable proton among all the samples) in the Supporting Information (Section S5.2, Figures S175–S176). With our new, higher quality experimental data, we confirmed the conformation which has been previously found[11,12] for the distal base in **1-Co-O_2**: the Euler rotation relating the *g*-tensor and the hyperfine coupling tensors A^H was found to be $[0°, 105°, 0°] \pm 10°$. The new data suggest a purely dipolar nature of the hyperfine coupling between the distal proton and the electron spin $A^H = [-6.5\ -6.5\ 13.0]$ MHz in contrast to the previous results in which a small isotropic

© 2016 Wiley-VCH Verlag GmbH & Co. KGaA, Weinheim

Table 1. Principal values of *g*- and *A*- interaction tensors for **1–6-Co-O_2** and **8-Co-O_2** determined with EasySpin from the Q-band ESE and Davies-ENDOR spectra. The distance between the distal proton and the electron spin was computed using the point dipolar approximation.[34] The corresponding data for **7-Co** could not be produced because no stable **7-Co-O_2** complex could be obtained. The data are presented in the order of increasing hyperfine coupling of the distal proton.

Compound	$[g_x\ g_y\ g_z]$	$[A_x\ A_y\ A_z]$ [MHz]	distal proton-e⁻ distance [Å]
1-Co-O_2	[2.0073 1.9920 2.0780]	[−6.5 −6.5 13.0]	2.30
3-Co-O_2	[2.0057 1.9920 2.0780]	[−6.5 −6.5 13.0]	2.30
2-Co-O_2	[2.0053 1.9925 2.0740]	[−6.6 −6.6 13.2]	2.29
6-Co-O_2	[2.0065 1.9910 2.0765]	[−6.9 −6.9 13.8]	2.25
5-Co-O_2	[2.0085 1.9920 2.0780]	[−7.0 −7.0 14.0]	2.24
4-Co-O_2	[2.0055 1.9910 2.0785]	[−7.2 −7.2 14.4]	2.22
8-Co-O_2	[2.0045 1.9900 2.0825]	–	–

contribution was reported.[11,12] Analysis of the experimental Davies-ENDOR data revealed that the conformation of the distal base in **1-Co-O_2**, which was found previously[11,12] and confirmed here, was preserved in the **1–6-Co-O_2** series (i.e. the same Euler rotation applies throughout) while the strength of the coupling varied. Principal values of the hyperfine coupling tensor of the strongly coupled distal proton in the **1–6-Co-O_2** series are summarized in Table 1. The data show that the strength of the hyperfine coupling of the distal proton increases as follows: **1-Co-O_2** ≈ **3-Co-O_2** < **2-Co-O_2** < **6-Co-O_2** < **5-Co-O_2** < **4-Co-O_2**. Accordingly, the distance between the distal proton and the electron spin, computed from the hyperfine coupling tensor of the distal proton using the point dipolar approximation,[32] decreases along the series (Table 1). This trend of the hyperfine coupling among the **1–6-Co-O_2** complexes was confirmed by adding up the Davies-ENDOR spectra acquired at different observer positions and analyzing the resulting sum Davies-ENDOR spectra (Figure 4). Such sum spectra do

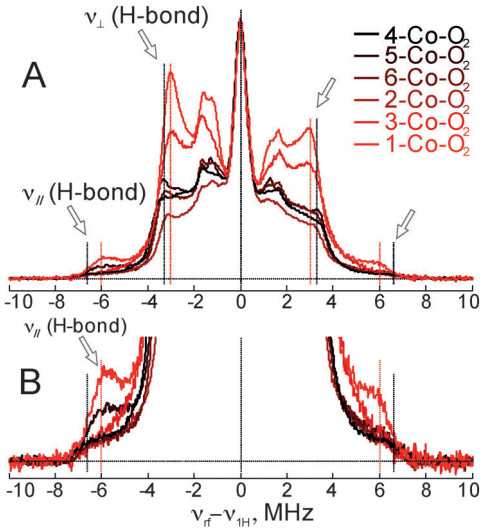

Figure 4. Summed Davies-ENDOR spectra for **1–6-Co-O_2** species (Q band, 10 K). A) Complete spectra. B) Spectra are shown at increased scale. Vertical dotted lines in (A) and (B) are added in order to facilitate visual comparison of the spectra.

not contain information on relative orientation of the hyperfine and the *g*-tensors, hence relative coupling strengths can be readily compared.

Regarding the **7-Co** complex, no stable **7-Co-O_2** species could be obtained. Hence, neither ESE nor Davies-ENDOR experiments could be performed in that case. With the **8-Co-O_2** complex, only one Davies-ENDOR spectrum could be acquired due to a very weak contribution from the strongly coupled proton that required an extremely long acquisition time. This prevented thorough characterization of the detected strong coupling in **8-Co-O_2** in terms of the strength and geometry (see the Supporting Information; Figure S183 and the accompanying text).

The present results show that the N–H acidity of the distal base has a decisive influence on the strength of the H-bond. Initial theoretical estimates of N–H acidity (more precisely—ACD-calculated pK_a[13] values) correlate well with the experimentally determined H-bond strength. Both suggest existence of two rather distinct groups of the compounds: one with a weaker coupling (**1-Co-O_2** ≈ **3-Co-O_2** < **2-Co-O_2**) and the other one with a stronger coupling (**6-Co-O_2** < **5-Co-O_2** < **4-Co-O_2**). Even though the predictions do not perfectly agree with experiment down to fine details (for instance, experimental data suggest stronger coupling in **3-Co-O_2** than in **2-Co-O_2** as well as the strongest coupling in **4-Co-O_2**), the inconsistencies between predictions and experimental findings are minor.

Conclusion

A series of model complexes **1–8-Co-O_2** for the dioxygen-binding site of Mb and Hb was synthesized in order to systematically study the strength of the H-bond between the distal residue and bound dioxygen. The key step in their preparation was the Sonogashira cross-coupling of porphyrin **10-Zn** with compounds **11–18** in the presence of [Pd(PPh_3)$_4$] as a catalyst. During the course of this reaction, apart from the formation of the desired model complex, porphyrin **9-Zn** was formed by transfer of a phenyl group from the PPh_3 ligand of the palladium catalyst to the metal and subsequent coupling to the acetylene moiety.

Based on ^{1}H NMR studies ($CHCl_3$, 25 °C), the alkyl-tethered imidazole (proximal residue) in complexes **1-Zn**, **2-Zn**, **4–6-Zn**, and **9-Zn** is axially ligated to the Zn^{II} ion and the distal residue is preferably rotated towards the porphyrin plane. In contrast, such conformational preferences could not be supported for complexes **7-Zn** and **8-Zn**. It is likely that, for these two porphyrins, there is a dynamic equilibrium between ligation of the proximal or the distal base to the central Zn^{II} ion, with rates that are comparable to the NMR timescale.

The hyperfine interaction between the dioxygen radical and neighboring exchangeable H-nucleus in **1–6-Co-O_2** was clearly resolved by Q-band Davies-ENDOR spectroscopy. We have shown that while the geometry of the hyperfine interaction (accompanied by the conformation of the distal base in the compounds) is preserved throughout the **1–6-Co-O_2** series, the strength of the interaction increases with increasing the N–H acidity of the distal base.

© 2016 Wiley-VCH Verlag GmbH & Co. KGaA, Weinheim

Experimental Section

General information

Porphyrins **1-Zn** and **10-Zn**,[11,12] benzimidazole **11**,[18a,33] 4-iodo-2-nitroaniline (**19**),[18] 3-fluoro-2-nitroaniline (**22**),[26] and 6-iodo-3-nitropyridin-2-amine (**26**)[29] were prepared according to known literature procedures. The Supporting Information (SI) contains: synthesis of porphyrin **10-Zn**; proposed mechanism for the formation of porphyrin **9-Zn**; synthetic procedures and spectral data of zinc porphyrins **2**–**9-Zn**, free-base porphyrins **1**–**9**–**2H**, cobalt porphyrins **1**–**9-Co**, iodinated distal base precursors **12**–**18**, and precursor compounds **19**–**27**; copies of UV/Vis spectra, 1D and 2D NMR spectra of all new compounds; X-band cw-EPR and Q-band Davies-ENDOR spectra.

EPR spectroscopy and spectral simulations

Continuous wave (cw) EPR experiments were performed at 120 K at X-band frequencies with a commercial X/W-band Elexsys E680 spectrometer equipped with an EN4118X-MD4-W1 probehead (both from Bruker). Spectra were acquired at 0.2012 mW incident microwave power with 0.2 mT modulation amplitude; the microwave resonator was critically coupled.

All pulse EPR experiments were performed at 10 K at Q band with a commercial X/Q-band Elexsys E580 spectrometer equipped with a EN 5107D2 Q-band resonator (both from Bruker). Electron spin echo detected field swept spectra (ESE spectra) were taken with the $\pi/2$ (40 ns) $-$ π (80 ns) primary echo sequence. Q-band Davies-ENDOR spectra were acquired using a conventional Davies-ENDOR pulse sequence.[34] The length of the preparation (π) pulse was 80 ns; for the detection "$\pi/2-\pi$" block 40 ns and 80 ns microwave pulses were used. Such excitation enhances appearance of the strongly coupled species in Davies-ENDOR spectra; it was found optimal for detection of the exchangeable protons in the previous studies.[11,12] To straighten the baseline, the stochastic acquisition mode was chosen for recording the Davies-ENDOR spectra. For every compound, Davies-ENDOR spectra were taken at many (13–21) observer positions of the ESE spectrum to allow for an accurate determination of the hyperfine interaction tensor of the strongly coupled exchangeable proton of the distal base. For all EPR measurements (both at X and Q bands) quartz sample tubes (Wilmad) with 1.6 mm outer diameter were used.

Spectral simulations were performed with EasySpin.[35] The spin system to simulate ESE spectra contained one electron ($S=1/2$) and one ^{59}Co nucleus ($I=7/2$). No further nuclei (e.g. protons) were taken explicitly into account, as they contribute mainly to the overall linewidth due to their weak hyperfine couplings. An analogous spin system was used previously.[11] The hyperfine coupling tensor of ^{59}Co was taken as $A^{Co}=[-54\ -28\ -28]$ MHz with the relative orientation with respect to the *g*-tensor described by the Euler angles (a, b, g)=(0°, 70°, 0°). These parameters were determined previously[11,12] and were left unchanged. For each compound, principal values of the *g*-tensors and line broadening parameters (defined as the *HS*-strain tensor) were varied in order to achieve the best possible visual match with experimental spectra. The spin system for simulating the Davies-ENDOR spectra contained one electron ($S=1/2$) and one nucleus ($I=1/2$) representing a strongly coupled proton. The hyperfine coupling tensor of the proton was expressed as $a_{iso} + a_T[-1\ -1\ 2]$ during the simulations. All experimental spectra were background-corrected prior to simulations. Best matching models were manually selected on the basis of the visual analysis rather than automated fitting with an *rmsd* criterion. We proceeded like this because of the complexity of the underlying spin system (high number of free parameters and complex line broadening mechanism) and the high complexity of the experimental spectra stemming from their rich content. The latter was especially the case for the Davies-ENDOR spectra.

Preparation of 1–8-Co-O_2 species

In order to prepare **1**–**8-Co-O_2** complexes for the Davies-ENDOR experiments, compounds **1**–**8-Co** were dissolved in a CH_2Cl_2/toluene 4:1 mixture under oxygen-free atmosphere in a glovebox, and were subsequently subjected to oxygenation. The process was controlled by monitoring relative intensities of signals from the oxygenated and the non-oxygenated species in the cw-EPR spectra at X band. The signal from the non-oxygenated species (**1**–**8-Co)** originates from a low-spin Co^{II} species in axial local surrounding.[11] After the oxygenation, the spin density is largely shifted on the dioxygen species of the oxygenated complex. The resulting EPR signal is significantly narrower and exhibits different spectral features. Importantly, it is located at higher magnetic fields (smaller *g*-factor range) with only minor overlap with the signal from the original non-oxygenated compound. Both types of signals were characterized previously.[11,12] Our first attempts to perform oxygenation by blowing a dioxygen stream from a balloon directly into the 3 mm o.d. EPR tube as discussed previously[11] showed poor control over the oxygenation process and led to oxidation beyond the desired **1**–**8-Co-O_2** species. In particular, a very strong drop of intensity of the cw-EPR spectrum from the sample after the oxygenation was always observed. In order to overcome this problem, milder oxygenation was performed with ambient air in smaller 1.6 mm o.d. EPR tubes with regular probing of the oxygenation extent by cw-EPR (for more details see Section S5.1 in the Supporting Information). Upon exposure to dioxygen, most of the **1**–**8-Co** compounds were initially oxygenated to the respective **1**–**8-Co-O_2** complexes (first phase) indicated by an increase in the signal intensity stemming from the dioxygen species, and then they underwent further transformations associated presumably with the formation of other paramagnetic Co^{II} complexes (second phase) accompanied by broadening and eventually deforming of the EPR signal. In the present work we refrained from in-depth studying of the oxygenation kinetics and focused on obtaining the primary oxygenated **1**–**8-Co-O_2** compounds in good quality.

The results of the mild oxygenation procedure are summarized in Figure S174 in the Supporting Information. For the **1**–**5-Co** compounds, the ratio between the signal intensities from the oxygenated to the non-oxygenated species was gradually increasing upon oxygenation (i.e. Figure S174 A) though a different oxygenating kinetics was observed in each case. It was generally difficult to reach a full oxygenation.

Prolonged oxygenation led to oxidation beyond the **1**–**5-Co-O_2** complex as indicated by a characteristic line broadening, Figure S174. Note that no signals from the strongly coupled protons could later be detected by Q-band ENDOR from such secondary-oxidized samples. Good **1-Co-O_2**, **2-Co-O_2**, **3-Co-O_2**, and **4**–**5-Co-O_2** complexes were obtained after 3, <1, 15, and 10 min of oxygenation, respectively. Unusually fast oxygenation kinetics was observed for **6-Co**; an undesired line broadening was seen already shortly after the oxygenation begun (Figure S174 B). Notably, a complete oxygenated **6-Co-O_2** sample was obtained by transferring the material into the EPR tube in the air rather than in the glovebox. Figure S174 (part C) shows EPR spectra from the desired **1**–**6-Co-O_2** complexes.

For compounds **7-Co** and **8-Co** (Figure 1), oxygenation/oxidation kinetics was much faster than in the other cases. For example, for

© 2016 Wiley-VCH Verlag GmbH & Co. KGaA, Weinheim

7-Co the secondary oxidation product was observed already in samples that were not intentionally exposed to air or oxygen at any time. For **8-Co**, we could obtain the **8-Co-O_2** complex only by transferring the material into the EPR tube in the air, as was similarly found in the case of **6-Co-O_2**. However, the relative content of the species featuring the strongly coupled proton, as was later revealed by Q-band ENDOR measurements, was extremely low. More details on the oxygenation of **7-Co** and **8-Co** are provided in Section S5.1 in the Supporting Information.

Acknowledgements

This work was supported by the Swiss National Science Foundation (SNF; grant number: 200021-140211). The research of M.N.A. is implemented within the framework of the Action "Supporting Postdoctoral Researchers" of the Operational Program "Education and Lifelong Learning" (Action's Beneficiary: General Secretariat for Research and Technology), and is co-financed by the European Social Fund (ESF) and the Greek State. The authors are especially grateful to Prof. Dr. Willem H. Koppenol and Dr. Reinhard Kissner for fruitful scientific discussions and for generously providing laboratory facilities. Dr. Henry Dube is gratefully acknowledged for valuable scientific discussions and suggestions and Dr. Bruno Bernet for help with the spectral interpretations. The authors also thank the ETH NMR service for acquiring some of the 1D/2D NMR spectra.

Keywords: dioxygen binding · ENDOR spectroscopy · heme proteins · hydrogen bond · model systems · NMR spectroscopy · porphyrins

[1] a) J. Vojtěchovský, K. Chu, J. Berendzen, R. M. Sweet, I. Schlichting, *Biophys. J.* **1999**, *77*, 2153 – 2174; b) E. L. Raven, A. G. Mauk, *Adv. Inorg. Chem.* **2000**, *51*, 1 – 50; c) J. R. H. Tame, B. Vallone, *Acta Crystallogr. Sect. D* **2000**, *56*, 805 – 811.

[2] a) M. D. Maines, *Annu. Rev. Pharmacol. Toxicol.* **1997**, *37*, 517 – 554; b) Y. Zhao, P. E. Brandish, D. P. Ballou, M. A. Marletta, *Proc. Natl. Acad. Sci. USA* **1999**, *96*, 14753 – 14758; c) K. Shikama, *Prog. Biophys. Mol. Biol.* **2006**, *91*, 83 – 162.

[3] a) J. S. Olson, R. E. McKinnie, M. P. Mims, D. K. White, *J. Am. Chem. Soc.* **1983**, *105*, 1522 – 1527; b) B. A. Springer, S. G. Sligar, J. S. Olson, G. N. Phillips, Jr., *Chem. Rev.* **1994**, *94*, 699 – 714; c) J. S. Olson, G. N. Phillips, Jr., *Biol. Inorg. Chem.* **1997**, *2*, 544 – 552; d) T. G. Spiro, P. M. Kozlowski, *Acc. Chem. Res.* **2001**, *34*, 137 – 144; e) G. S. Kachalova, A. N. Popov, H. D. Bartunik, *Science* **1999**, *284*, 473 – 476; f) J. P. Collman, R. Boulatov, C. J. Sunderland, L. Fu, *Chem. Rev.* **2004**, *104*, 561 – 588; g) J. S. Olson, A. Ghosh, in *The Smallest Biomolecules: Diatomics and their Interactions with Heme Proteins* (Ed.: A. Ghosh), Elsevier, London, **2008**, pp. 3 – 17.

[4] L. Pauling, *Nature* **1964**, *203*, 182 – 183.

[5] a) T. Yonetani, H. Yamamoto, T. Iizuka, *J. Biol. Chem.* **1974**, *249*, 2168 – 2174; b) M. Ikeda-Saito, T. Iizuka, H. Yamamoto, F. J. Kayne, T. Yonetani, *J. Biol. Chem.* **1977**, *252*, 4882 – 4887; c) M. Ikeda-Saito, H. Hori, T. Inubushi, T. Yonetani, *J. Biol. Chem.* **1981**, *256*, 10267 – 10271.

[6] a) T. Kitagawa, M. R. Ondrias, D. L. Rousseau, M. Ikeda-Saito, T. Yonetani, *Nature* **1982**, *298*, 869 – 871; b) K. Nagai, B. Luisi, D. Shih, G. Miyazaki, K. Imai, C. Poyart, A. De Young, L. Kwiatkowsky, R. W. Noble, S.-H. Lin, N.-T. Yu, *Nature* **1987**, *329*, 858 – 860.

[7] a) J. Mispelter, M. Momenteau, D. Lavalette, J.-M. Lhoste, *J. Am. Chem. Soc.* **1983**, *105*, 5165 – 5166; b) J. A. Lukin, V. Simplaceanu, M. Zou, N. T. Ho, C. Ho, *Proc. Natl. Acad. Sci. USA* **2000**, *97*, 10354 – 10358.

[8] S. E. V. Phillips, B. P. Schoenborn, *Nature* **1981**, *292*, 81 – 82.

[9] a) S. E. V. Phillips, *J. Mol. Biol.* **1980**, *142*, 531 – 554; b) F. Yang, G. N. Phillips, Jr., *J. Mol. Biol.* **1996**, *256*, 762 – 774; c) S.-Y. Park, T. Yokoyama, N. Shibayama, Y. Shiro, J. R. H. Tame, *J. Mol. Biol.* **2006**, *360*, 690 – 701.

[10] I. Birukou, R. L. Schweers, J. S. Olson, *J. Biol. Chem.* **2010**, *285*, 8840 – 8854.

[11] H. Dube, B. Kasumaj, C. Calle, M. Saito, G. Jeschke, F. Diederich, *Angew. Chem. Int. Ed.* **2008**, *47*, 2600 – 2603; *Angew. Chem.* **2008**, *120*, 2638 – 2642.

[12] H. Dube, B. Kasumaj, C. Calle, B. Felber, M. Saito, G. Jeschke, F. Diederich, *Chem. Eur. J.* **2009**, *15*, 125 – 135.

[13] ACD/Percepta, version 14.0.0, Advanced Chemistry Development, Inc., Toronto, ON, Canada, 2014, www.acdlabs.com (accessed April 1, 2015). For predicting and tuning the pK_a values of basic amine centers, see: M. Morgenthaler, E. Schweizer, A. Hoffmann-Röder, F. Benini, R. E. Martin, G. Jaeschke, B. Wagner, H. Fischer, S. Bendels, D. Zimmerli, J. Schneider, F. Diederich, M. Kansy, K. Müller, *ChemMedChem* **2007**, *2*, 1100 – 1115.

[14] Due to the instability of **2**–**8**-**Zn**, their purification proved to be very challenging. In particular, these porphyrins were purified by FC in the dark (SiO_2; solvent, 1% v/v Et_3N) and preparative GPC (Jaigel-2H and NovoGROM 500 or Bio-Beads SX-1).

[15] For the formation of scrambled products under Sonogashira and Suzuki cross-coupling conditions, see: a) R. W. Wagner, Y. Ciringh, C. Clausen, J. S. Lindsey, *Chem. Mater.* **1999**, *11*, 2974 – 2983; b) M. Kozaki, S. Morita, S. Suzuki, K. Okada, *J. Org. Chem.* **2012**, *77*, 9447 – 9457; c) M. N. Alberti, S. Nowakowska, M. D. Tzirakis, J. Nowakowski, P. Fesser, W. B. Schweizer, A. Shchyrba, C. Thilgen, T. A. Jung, F. Diederich, *Eur. J. Org. Chem.* **2014**, 5705 – 5719.

[16] F. E. Goodson, T. I. Wallow, B. M. Novak, *J. Am. Chem. Soc.* **1997**, *119*, 12441 – 12453.

[17] a) C.-z. Li, K. Nishiyama, I. Taniguchi, *Electrochim. Acta* **2000**, *45*, 2883 – 2888; b) M. C. Marden, L. Kiger, C. Poyart, A. K. Rashid, J. Kister, F. Stetzkowski-Marden, G. Caron, M. Haque, L. Moens, *FEBS Lett.* **2000**, *472*, 221 – 224.

[18] a) J. G. Wilson, F. C. Hunt, *Aust. J. Chem.* **1983**, *36*, 2317 – 2325; b) F. Maya, J. M. Tour, *Tetrahedron* **2004**, *60*, 81 – 92.

[19] For the synthesis of benzimidazoles from *o*-nitroanilines and aldehydes in one step by a reductive cyclization, see: D. Yang, D. Fokas, J. Li, L. Yu, C. M. Baldino, *Synthesis* **2005**, 47 – 56.

[20] M. Belema, A. C. Good, J. Goodrich, R. Kakarla, G. Li, O. D. Lopez, V. N. Nguyen, J. Kapur, Y. Qiu, J. L. Romine, D. R. St. Laurent, M. Serrano-Wu, L. B. Snyder, F. Yang (Bristol-Myers Squibb Company), PCT. Int. Appl. WO 2010/017401 A1, **2010**.

[21] For a general method of the synthesis of 2-(trifluoromethyl)-1*H*-benzimidazoles, see: G. Navarrete-Vázquez, M. M. Rojano-Vilchis, L. Yépez-Mulia, V. Meléndez, L. Gerena, A. Hernández-Campos, R. Castillo, F. Hernández-Luis, *Eur. J. Med. Chem.* **2006**, *41*, 135 – 141.

[22] M. J. Wythes, M. J. Palmer, M. I. Kemp, M. C. Mackenny, R. J. Maguire, J. F. Blake, Jr., PCT Int. Appl. WO 2000/05231A1, **2000**.

[23] P. K. Dubey, A. Naidu, V. Anandam, G. Hemasunder, *Indian J. Chem. Sect. B* **2005**, *44*, 1239 – 1242.

[24] M. Andrzejewska, M. A. Pagano, F. Meggio, A. M. Brunati, Z. Kazimierczuk, *Bioorg. Med. Chem.* **2003**, *11*, 3997 – 4002.

[25] E. E. Simanek, A. Tsoi, C. C. C. Wang, G. M. Whitesides, M. T. McBride, G. T. R. Palmore, *Chem. Mater.* **1997**, *9*, 1954 – 1961.

[26] C. J. Diaz, C. D. Haffner, J. D. Speake, C. Zhang, W. Y. Mills, P. K. Spearing, D. J. Cowan, G. M. Green PCT Int. Appl. WO 2008/021851A2, **2008**.

[27] a) D. A. Nugiel, K. Jacobs, L. Cornelius, C.-H. Chang, P. K. Jadhav, E. R. Holler, R. M. Klabe, L. T. Bacheler, B. Cordova, S. Garber, C. Reid, K. A. Logue, L. J. Gorey-Feret, G. N. Lam, S. Erickson-Viitanen, S. P. Seitz, *J. Med. Chem.* **1997**, *40*, 1465 – 1474; b) M. von Wantoch Rekowski, A. Pyriochou, N. Papapetropoulos, A. Stößel, A. Papapetropoulos, A. Giannis, *Bioorg. Med. Chem.* **2010**, *18*, 1288 – 1296.

[28] K. F. Ansari, C. Lal, *Eur. J. Med. Chem.* **2009**, *44*, 4028 – 4033.

[29] B. C. Askew, M. J. Breslin, M. E. Duggan, J. H. Hutchinson, R. S. Meissner, J. J. Perkins, T. G. Steele, M. A. Patane, PCT Int. Appl. WO 2001/53262A1, **2001**.

[30] P. Weyermann, F. Diederich, *Helv. Chim. Acta* **2002**, *85*, 599 – 617.

[31] a) H. Adams, K. D. M. Harris, G. A. Hembury, C. A. Hunter, D. Livingstone, J. F. McCabe, *Chem. Commun.* **1996**, 2531 – 2532; b) C. Allott, H. Adams, P. L. Bernad, Jr., C. A. Hunter, C. Rotger, J. A. Thomas, *Chem. Commun.*

© 2016 Wiley-VCH Verlag GmbH & Co. KGaA, Weinheim

1998, 2449 – 2450; c) E. A. Meyer, R. K. Castellano, F. Diederich, *Angew. Chem. Int. Ed.* **2003**, *42*, 1210 – 1250; *Angew. Chem.* **2003**, *115*, 1244 – 1287; d) L. M. Salonen, M. Ellermann, F. Diederich, *Angew. Chem. Int. Ed.* **2011**, *50*, 4808 – 4842; *Angew. Chem.* **2011**, *123*, 4908 – 4944.

[32] A. Schweiger, G. Jeschke, *Principles of Pulse Electron Paramagnetic Resonance*, Oxford University Press, Oxford, **2001**.

[33] Z. Kazimierczuk, L. Dudycz, R. Stolarski, D. Shugar, *J. Carbohydr. Nucleosides Nucleotides* **1981**, *8*, 101 – 117.

[34] a) C. Fan, P. E. Doan, C. E. Davoust, B. M. Hoffman, *J. Magn. Reson.* **1992**, *98*, 62 – 72; b) E. R. Davies, *Phys. Lett. A* **1974**, *47*, 1 – 2.

[35] S. Stoll, A. Schweiger, *J. Magn. Reson.* **2006**, *178*, 42 – 55.

Received: March 31, 2016
Published online on ■■ ■■, 0000

© 2016 Wiley-VCH Verlag GmbH & Co. KGaA, Weinheim

FULL PAPER

Hydrogen Bonds

M. N. Alberti, Y. Polyhach, M. D. Tzirakis, L. Tödtli, G. Jeschke, F. Diederich**

■■ – ■■

Exploring the Strength of the H-Bond in Synthetic Models for Heme Proteins: The Importance of the N–H Acidity of the Distal Base

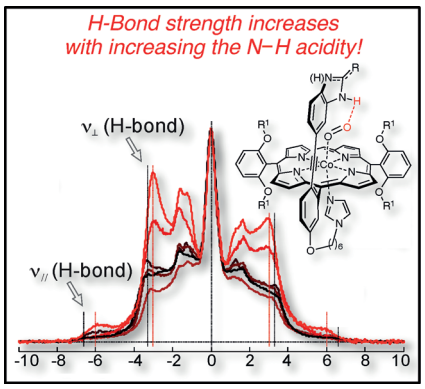

The distal hydrogen bond in dioxygen-binding proteins is crucial for the discrimination of O_2 with respect to CO or NO. The H-bond donor ability of distal heterocycles, as predicted based on pK_a values, has been varied systematically. The H-bond in the dioxygen adducts of the Co^{II} porphyrins was directly measured by Q-band Davies-ENDOR spectroscopy, and it was shown that the strength of the hyperfine coupling between the dioxygen radical and the distal H-atom increases with enhanced acidity of the H-bond donor.

© 2016 Wiley-VCH Verlag GmbH & Co. KGaA, Weinheim